Visualization of hydraulic cylinder dynamics by a structure preserving nondimensionalization

Satoru Sakai, *Member, IEEE* and Stefano Stramigioli, *Fellow, IEEE*

***Abstract*—This paper reveals a new simplicity of a nominal hydraulic cylinder model whose original representation suffers from too many physical parameters. The 8-dimensional parameter space in the original representation is reduced to a 3-dimensional parameter space in the proposed nondimensional representation while preserving the parametric structure. To clarify comprehensive relations between the nonlinear dynamics and the many physical parameters, an advanced direct search approach is suggested. More precisely, we can repeat the fast computation of the nonlinear dynamics and the updates of only three parameters without verifying any new simulator. The efficient visualization of the numerical solutions presents the best possible result corresponding to the analytical solution.**

***Index Terms*—Hydraulic systems, nonlinear dynamics, fast computation, visualization.**

I. Introduction

Balance between accuracy and simplicity is a key in modeling for control of hydraulic cylinders. Hydraulic cylinders are a fluid-mechanical system. However, instead of the infinite dimensional model, which achieves high accuracy, the finite dimensional nominal models are accepted in many controller design procedures [1] [2] [3] [4]. Nevertheless, such nominal models are still complex in terms of not only the nonlinear dynamics (nonlinear response) but also the many physical parameters in the original representation. In fact, in addition to the well-known mechanical parameters such as the damping constant, the several fluid parameters such as the bulk modulus and the source pressure can be dominant in the nonlinear response [5] [6]. Eventually, the comprehensive relations between the nonlinear dynamics and the many physical parameters are not entirely clarified. This implies that even if a good control result is achieved under a certain experimental condition, it may not be justifiable to apply the result to more general conditions. For example, when a linearization based control [7] is useful for a certain experimental hydraulic system, it is not clear when the linearization is useful again for other hydraulic systems.

To overcome this situation, due to the nonlinear response, numerical studies are important and relevant. However, since the original parameter space is too large due to the many physical parameters, it is never efficient to apply the conventional direct search (the brute-force search) approaches [8] in which the computation of the nonlinear dynamics and the updates of the many physical parameters are repeated in the original representation. Also, even if the original parameter space is reduced by an usual nondimensional representation, it is never efficient to build and verify a new simulator for the usual nondimensional representation where the existing simulator for the original representation cannot be applied.

On the other hand, such comprehensive relations are already studied for other systems. The mass-damper-spring

$$m\frac{d^2s}{dt^2} + d\,\frac{ds}{dt} + ks = f$$

in the original representation is transformed to

$$\ddot{s}^* + d^*\dot{s}^* + s^* = f^*$$

in a special nondimensional representation with only one parameter $d^* = d/\sqrt{mk}$ preserving the parametric structure and the analytical study completely clarified the relations (e.g., the critical response at $d^* = 2$) based on the linearity. The Navier-Stokes equations of a fluid system [9]

$$\frac{\partial u}{\partial t} + (u \cdot \nabla)u = -\frac{1}{\rho}\nabla p + ge_g + \nu\Delta u$$

in the original representation is transformed to

$$\frac{\partial u^*}{\partial t^*} + (u^* \cdot \nabla^*)u^* = -\nabla^* p^* + \frac{1}{\mathrm{Fr}^2}e_g^* + \frac{1}{\mathrm{Re}}\Delta^* u^*$$

in a special nondimensional representation with only two parameters Fr and Re preserving the parametric structure and many numerical studies have clarified the relations. These analytical and numerical studies which are not detailed here provide the foundations for many things today.

To clarify such relations for a nominal hydraulic cylinder model as well, this paper proposes a new special nondimensional representation that preserves the parametric structure and suggests an advanced direct search approach different from the conventional ones with respect to both the efficiency and visualization (3D-visualization), without which many numerical studies are less valuable. The proposed nondimensional representation is a new simplicity of the nominal model that does not exist in more accurate or complex existing models (e.g. [10] [11] in the original representation) as well as in the merely simple (freely-truncated) existing models. More precisely, without building and verifying any new simulator, we can repeat the fast computation of the nonlinear dynamics and the updates of only three parameters in the proposed nondimensional representation. To provide an example, the numerical existence and nonlinearity are efficiently visualized

Manuscript received September 1, 201x; revised June 2x, 201x. This work was supported by JSPS KAKENHI JP26420173 and Fluid Power Technology Promotion Foundation. XXXXXXXXXXXXXXXXXXXXXXXXXXXXXXX XXXXXXXXXXXXXXXXXXXXXXXXXXXXXX XXXXXXXXXXXXXXXXXXXXXXXXXXXXXX XXXXXXXXXXXXXXXXXXXXXXXXXXXXXX

Satoru Sakai is with Faculty of Mechanical Engineering, Shinshu University, Japan. Stefano Stramigioli is with Faculty of Electrical Engineering, University of Twente, Netherlands.

since the nonlinear dynamics computations are impossible if the numerical existence is not achieved and the linearization is less reliable if the nonlinearity is strong.

The rest of this paper is organized as follows. In Section II, a nominal model of hydraulic cylinders is reviewed in the original representation. A new special nondimensional representation is proposed and compared with other nondimensional representations in Section III. In Section IV, the effectiveness of the proposed nondimensional representation is confirmed. Conclusions are provided in Section V.

II. The Nominal Model

Let us start with the nominal model of Figure 1 in the original representation: [12] [13] [14] [15]

$$\Sigma_0 \begin{cases} M\dfrac{d^2s}{dt^2} = -D\dfrac{ds}{dt} + A_+p_+ - A_-p_- \\ \dfrac{dp_+}{dt} = \dfrac{b}{A_+(L/2+s(t))}\left[-A_+\dfrac{ds}{dt} + Q_+(p_+,u)\right] \\ \dfrac{dp_-}{dt} = \dfrac{b}{A_-(L/2-s(t))}\left[+A_-\dfrac{ds}{dt} - Q_-(p_-,u)\right] \end{cases} \quad (1)$$

where the displacement $s(t)$ [m], the cap pressure $p_+(t)$ [Pa], the rod pressure $p_-(t)$ [Pa], and the spool displacement (the input) $u(t)$ [m] are the functions of time t [s]. The subscript $+$ and $-$ denote the cap-side and the rod-side, respectively, and the subscript $\pm$ denotes both sides. The driving force is $f(t) = A_+p_+(t) - A_-p_-(t)$ [N]. The mass M [kg], the damping constant D [Ns/m], the piston areas $A_+ \geq A_-$ [m^2], and the bulk modulus b [Pa] are the positive constants. The cylinder volumes $V_+(s(t)) := A_+(L/2+s(t)), V_-(s(t)) := A_-(L/2-s(t))$ [m^3] with the constant stroke L [m] are the functions of the displacement $s(t)$. The input flows Q_+ and Q_- [m^3/s], are approximated by Bernoulli's principle:

$$Q_+ = B(p_+, +u)u, \quad Q_- = B(p_-, -u)u \quad (2)$$

with

$$B(r,u) = \begin{cases} C\sqrt{-r+P} & (u>0) \\ 0 & (u=0) \\ C\sqrt{+r-0} & (u<0) \end{cases}$$

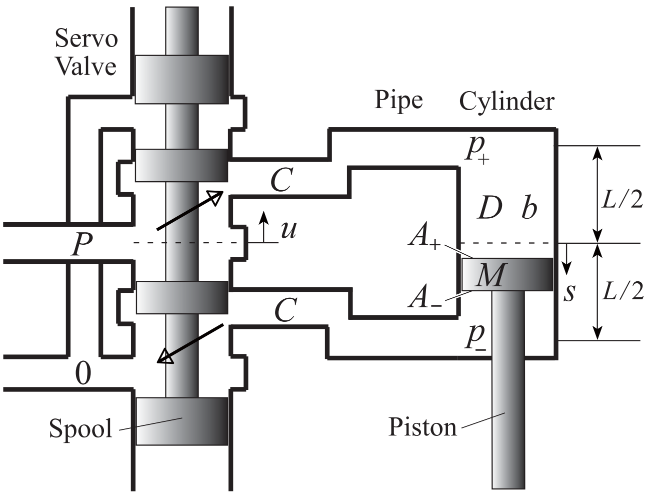

Fig. 1. Nominal hydraulic cylinder model.

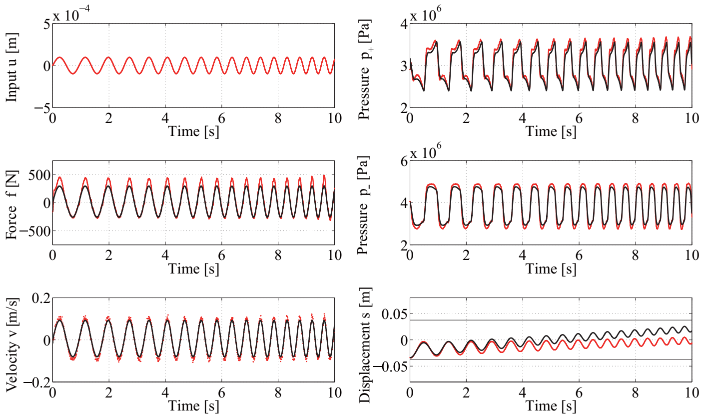

Fig. 2. Example of the nominal model output (the black curves) with $(M, D, L, A_+, A_-, b, C, P) = (14, 3200, 0.075, 7.0\times10^{-4}, 5.4\times10^{-4}, 5.3\times10^{8}, 1.6\times10^{-4}, 7\times10^{6})$ and the experimental output [15] (the red dots) whose valve is replaced by LSVG-01EH-20-WC-A1-10 (Yuken Kogyo).

where the flow gain C [$\sqrt{\mathrm{m}^5/\mathrm{kg}}$] and the source pressure P [Pa] are the positive constants. The nominal model introduces the restricted domain $s \in (-L/2, L/2)$ and $p_\pm \in [0, P]$ and the absolute notation within the square root functions (2) is dropped.

Remark 1 (Relating to uncertainty) The equations (1) ignore the nonlinear friction effect and also the internal and external leakage effects at least. The equations (2) assume the steady flow and the negligible servo dynamics of the zero-lapped spool valve. On the other hand, the stroke L can include the pipeline length effect and the bulk modulus b includes the pipeline (or tube) flexibility effect. Figure 2 shows an example of the accuracy between the nominal model (1) (2) and an experimental setup (a real system) in a practical frequency band (see [15] for details). This figure displays a long time cross validation in which the experimental outputs (the red dots) were never used in the parameter identification procedure for the nominal model outputs (the black curves). Nevertheless, with respect to the nonlinear responses in the pressures and displacement, the nominal model has an accuracy that any linearized model (transfer function) cannot have. Of course, the difference (e.g. the nonlinear friction effect) between the nominal model and the experimental setup exists and depends on each experimental setup but would change continuously. In the context of robust control [16] [17], the difference is uncertainty taken into account in the controller design procedure.

The nominal model (1) (2) is not our result. Not the accuracy but a new simplicity is our contribution evaluated in terms of the efficiency and visualization.

III. A Special Nondimensionalization

First, a new special nondimensional representation is proposed. Second, the advantages of the proposed nondimensional representation are discussed in comparison with other nondimensional ones because they are not unique [18] [19].

Proposition 1 (Special nondimensional representation) *Consider the original representation (1) (2) of the nom-*

inal model. Then, there exists a set of a time scaling $t^* = (1/T)t$, a variable scaling $(s^*, p_+^*, p_-^*)^{\mathrm{T}} = ((1/S)s, (1/P_+)p_+, (1/P_-)p_-)^{\mathrm{T}}$, and an input scaling $u_* = (1/U)u$ by which the original representation (1) (2) is transformed to the following nondimensional representation:

$$\Sigma_s \begin{cases} \ddot{s}^* = -D^*\dot{s}^* + p_+^* - A^* p_-^* \\ \dot{p}_+^* = \dfrac{1}{1/2+s^*}\left(-\dot{s}^* + Q_+^*\right) \\ \dot{p}_-^* = \dfrac{1}{1/2-s^*}\left(+\dot{s}^* - \dfrac{1}{A^*}Q_-^*\right) \end{cases} \tag{3}$$

and

$$Q_+^* = B^*(p_+^*, +u^*)u^*, \quad Q_-^* = B^*(p_-^*, -u^*)u^* \tag{4}$$

with

$$B^*(r,u) = \begin{cases} \sqrt{-r+P^*} & (u>0) \\ 0 & (u=0) \\ \sqrt{+r-0} & (u<0) \end{cases}$$

where T, S, P_+, P_-, and U are the constants and D^*, A^*, and P^* are the nondimensional parameters. The notation $\dot{\bullet}$ denotes the derivative with respect to the nondimensional time t^*.

In the following proof of Proposition 1, the original representation (1) (2) is converted into an input-state equation of a physical form from which the special nondimensional representation (3) (4) is derived via a set of the state and input transformation [20] and also the time transformation.

Proof of Proposition 1. The original representation (1) (2) is converted into an input-state equation of the form [13]:

$$\begin{cases} \dfrac{dx}{dt} = \underbrace{\begin{bmatrix} 0 & +1 & 0 & 0 \\ -1 & -D & J_{23} & J_{24} \\ 0 & -J_{23} & 0 & 0 \\ 0 & -J_{24} & 0 & 0 \end{bmatrix}}_{F} \nabla_x H + \underbrace{\begin{bmatrix} 0 \\ 0 \\ +bV_+^{-1}Q_+ \\ -bV_-^{-1}Q_- \end{bmatrix}}_{gu} \\ y = g^{\mathrm{T}}\nabla_x H \end{cases} \tag{5}$$

with the state $x = (s, p_m, p_+, p_-)^{\mathrm{T}}$,

$$J_{23}(s) = +bV_+(s)^{-1}A_+, \quad J_{24}(s) = -bV_-(s)^{-1}A_-,$$

and the original energy

$$H = p_m^2/(2M) - V_+(s)(b+p_+) - V_-(s)(b+p_-).$$

Here, the notation ∇_x denotes the gradient with respect to the variable x. The variable $p_m = Mv$ is the momentum imparted by the velocity $v = \frac{ds}{dt}$. By the gradient of the original energy H in the input-state equation of the form (5), the equations (1) are obtained by a direct calculation.

Since the state x is defined, let us take the set of the time transformation $t^* = (1/T)t$ with $T = \sqrt{(ML)/(bA_+)} =: T_s$, the state transformation $x^* = (s^*, v^*, p_+^*, p_-^*)^{\mathrm{T}} = X_s^{-1}x$ with

$$X_s := \begin{bmatrix} S & 0 & 0 & 0 \\ 0 & MS/T & 0 & 0 \\ 0 & 0 & P_+ & 0 \\ 0 & 0 & 0 & P_- \end{bmatrix} = \begin{bmatrix} L & 0 & 0 & 0 \\ 0 & \sqrt{MLbA_+} & 0 & 0 \\ 0 & 0 & b & 0 \\ 0 & 0 & 0 & b \end{bmatrix},$$

and the input transformation $u_* = (1/U)u$ with $U = (\sqrt{A_+^3 L/M})/C =: U_s$. Then the original form (5) is transformed to the nondimensional form:

$$\begin{cases} \dot{x}^* = \underbrace{\begin{bmatrix} 0 & +1 & 0 & 0 \\ -1 & -D^* & J_{23}^* & J_{24}^* \\ 0 & -J_{23}^* & 0 & 0 \\ 0 & -J_{24}^* & 0 & 0 \end{bmatrix}}_{T_s X_s^{-1} F X_s^{-T}} \nabla_{x^*} H^* + \underbrace{\begin{bmatrix} 0 \\ 0 \\ +J_{23}^* Q_+^* \\ -(J_{24}^*/A^*)Q_-^* \end{bmatrix}}_{T_s X_s^{-1} gUu^* =: g^* u^*} \\ y^* := g^{*\mathrm{T}} \nabla_{x^*} H^* \end{cases} \tag{6}$$

with

$$J_{23}^* = +1/(1/2+s^*), \quad J_{24}^* = -1/(1/2-s^*),$$

and the nondimensional energy

$$\begin{aligned} H^* &= (1/2)(v^*)^2 \\ &\quad -(1/2+s^*)(+1+p_+^*) \\ &\quad -(1/2-s^*)(+1+p_-^*)A^* \end{aligned}$$

in which $D^* := D\sqrt{L/(MbA_+)}$, $A^* := A_-/A_+$, $P^* := P/b$. Again, by the gradient of the nondimensional energy H^* in the input-state equation of the nondimensional form (6), the nondimensional representation (3) (4) is obtained. ■

In general, a model is valuable when the model has desirable properties that the other models do not have. Not only accuracy but also simplicity for control are among the properties. In a word, this paper highlights that the nominal model has high simplicity that more accurate or complex existing models (e.g., [10][11][21]) do not have as well as the merely simple (freely-truncated) existing models do not. A simplicity for control of the nominal model is the form (5) which is not our contribution and an application [13] of the physical form [22] [23] developed for the finite dimensional version of physical systems. The physical form provides so many links to fruitful results in modeling and control (e.g., modeling of the infinite dimensional systems, robust stabilization, learning) [24] [25] [26] than the general nonlinear forms (e.g., $\dot{x} = f(x) + g(x)u$ and $y = h(x)$ [27]). Indeed, the physical form is a special case of the general nonlinear forms. Regarding our contribution, the rest of this paper reveals that the nominal model has another simplicity for the parametric structure linked to the several advantages, that is, the efficiency and visualization.

Technically speaking, the proposed nondimensional representation (3) (4) is different from the conventional ones with respect to the visualization (3D-visualization) at a minimum. The time scaling in the famous nondimensionalizations [21] is not coupled with the state and input scaling to reduce the parameters for the visualization. Unlike the translational joint corresponding to the nominal model, the rotational joint [28] is complex due to more parameters making the visualization impossible. Also, the translational joint formulation cannot be a special case of the rotational joint formulation [29].

The first advantage of the proposed nondimensional representation (3) (4) is the parameter space reduction. The 8-dimensional parameter space with $\theta := (M, D, L, A_+, A_-, b, C, P) \in \mathbb{R}_+^8$ in the original representation (1) (2) is reduced to the 3-dimensional parameter space with $\theta^* := (D^*, A^*, P^*) \in \mathbb{R}_+ \times (0,1] \times \mathbb{R}_+ \subset \mathbb{R}_+^3 \subset \mathbb{R}_+^8$

in the proposed nondimensional representation (3) (4). Of course, other nondimensional representations bring a similar advantage [18] [19]. To discuss the additional advantages of the proposed nondimensional representation (3) (4), let us make our examples of other nondimensional representations.

Example 1 For the original physical form (5), let us take the set of the time transformation $t^* = (1/T)t$ with $T = \sqrt{(ML)/(bA_+)} =: T_1$ and the state transformation $x^* = (s^*, v^*, p_+^*, p_-^*)^{\mathrm{T}} = X_1^{-1}x$ with

$$X_1 := \begin{bmatrix} S & 0 & 0 & 0 \\ 0 & MS/T & 0 & 0 \\ 0 & 0 & P_+ & 0 \\ 0 & 0 & 0 & P_- \end{bmatrix} = \begin{bmatrix} L & 0 & 0 & 0 \\ 0 & \sqrt{MLbA_+} & 0 & 0 \\ 0 & 0 & b & 0 \\ 0 & 0 & 0 & bA_+/A_- \end{bmatrix}$$

and the input transformation $u_* = (1/U)u$ with $U = (\sqrt{A_+^3 L/M})/C =: U_1$. Then, via a procedure similar to the one in the proof of Proposition 1, we obtain one of the other nondimensional representations:

$$\Sigma_1 \begin{cases} \ddot{s}^* = -D^*\dot{s}^* + p_+^* - p_-^* \\ \dot{p}_+^* = \dfrac{1}{1/2 + s^*}\left(-\dot{s}^* + Q_+^*\right) \\ \dot{p}_-^* = \dfrac{1}{1/2 - s^*}\left(+A^*\dot{s}^* - \dfrac{1}{\sqrt{A^*}}Q_-^*\right) \end{cases} \tag{7}$$

and

$$Q_+^* = B^*(p_+^*, +u^*)u^*, \quad Q_-^* = B^*(p_-^*, -u^*)u^* \tag{8}$$

with

$$B^*(r, u^*) := \begin{cases} \sqrt{-r + P^*} & (u^* > 0) \\ 0 & (u^* = 0) \\ \sqrt{+r - 0} & (u^* < 0) \end{cases}$$

in which $D^* := D\sqrt{L/(MbA_+)}$, $A^* := A_-/A_+$, $P^* := P/b$. □

A significant difference between the nondimensionalizations in Proposition 1 and Example 1 is a parametric structure. By dropping the superscript $\bullet^*$, the proposed nondimensional representation (3) (4) can be equal to the original representation (1) (2) when $\theta = (1, D, 1, 1, A, 1, 1, P) \in \mathbb{R}_+^8$. However, by dropping the superscript $\bullet^*$, one of the other nondimensional representations (7) (8) generally *cannot* be equal to the original representation (1) (2). More precisely, the first equation in (7) can be equal to the first equation in (1) when $M = A_+ = A_- = 1$. The second equation in (7) can be also equal to the second equation in (1) when $L = A_+ = b = 1$. However, even if $L = A_- = b = 1$, the third equation in (7) cannot be equal to the third equation in (1) since $A^* \not\equiv 1$ for any C and P. In this sense, the other nondimensional representation (7) (8) fails to preserve the parametric structure in the original representation (1) (2) whereas the proposed nondimensionalization (3) (4) preserves it successfully. This difference can also be easily observed in the energy. The nondimensional energy in the other nondimensional representation (7) (8) is described by

$$\begin{aligned} H^* &= (1/2)(v^*)^2 \\ &\quad -(1/2 + s^*)(+1 + p_+^*) \\ &\quad -(1/2 - s^*)(+1 + p_-^*/A^*)A^*, \end{aligned}$$

and the parametric structure differs from that of the original energy H since $A^* \not\equiv 1$.

Eventually, the above significant difference is trivially rephrased as the following time response property of the hydraulic cylinders. Let the notation $\phi[\theta, x(0), u(t)]$ denote the state $x(t)$ in the original representation (1) (2) of $\theta = (M, D, L, A_+, A_-, b, C, P)$ at time t starting from the initial state $x(0)$ in the presence of the input signal $u(\tau)$ $(0 \le \tau \le t)$.

Theorem 1 (Structure preserving property) *Suppose the state $x(t) = \phi[\theta, x(0), u(t)]$ exists. Then the nondimensional state $x^*(t^*) = X_s^{-1}\phi[\theta, X_s x^*(0), U_s u^*(T_s t^*)]$ in the special nondimensional representation (3) (4) at nondimensional time $t^* = (1/T_s)t$ starting from the nondimensional initial state $x^*(0) = X_s^{-1}x(0)$ in the presence of the nondimensional input $u^*(t^*) = (1/U_s)u(t^*)$ is given as*

$$x^*(t^*) = \phi[\theta^*_{\mathrm{special}}(\theta), x^*(0), u^*(t^*)] \tag{9}$$

of $\theta^*_{\mathrm{special}}(\theta) = (1, \underbrace{D\sqrt{L/(MbA_+)}}_{0<D^*}, 1, 1, \underbrace{A_-/A_+}_{0<A^*\le 1}, 1, 1, \underbrace{P/b}_{0<P^*})$.

The second advantage is the verification-free based on Theorem 1. The existing simulator for the original representation (1) (2) cannot be applied as a simulator for the other nondimensionalization (7) (8). It is never efficient to build a new simulator for the other nondimensional representation. Moreover, from a practical viewpoint, the verification (e.g., checking of the simulator codes or settings) is more laborious than the building. But, based on Theorem 1, the existing simulator for the original representation (1) (2) is successfully applicable as a simulator for the proposed nondimensional representation (3) (4). Then we do not have to endure the verification. u The third advantage is the fast computation based on Theorem 1. The computation time for $x(t) = X_s\phi[\theta^*_{\mathrm{special}}(\theta), x^*(0), u^*(t/T_s)]$ should be shorter than that for $x(t) = \phi[\theta, x(0), u(t)]$. This is because the number of multiplication and division operations for the forward dynamics computations of (3) (4) is trivially small due to the unity parameters $(M, A_+, L, b, C) = (1, 1, 1, 1, 1)$ in equation (9) whereas the parametric structure in the original representation (1) (2) is preserved. Of course, computer performances has much improved since 1990' [29]. However, depending on the objective (e.g., numerical study or design optimization), the computation time is still substantial when many dynamics computations need to be repeated.

The fourth advantage of the proposed nondimensional representation is discussed after our next example.

Example 2 For the original physical form (5), let us take the set of the time transformation $t^* = (1/T)t$ with $T = \sqrt{M/(PL)} =: T_2$ and the state transformation $x^* = (s^*, v^*, p_+^*, p_-^*)^{\mathrm{T}} = X_2^{-1}x$ with

$$X_2 := \begin{bmatrix} S & 0 & 0 & 0 \\ 0 & MS/T & 0 & 0 \\ 0 & 0 & P_+ & 0 \\ 0 & 0 & 0 & P_- \end{bmatrix} = \begin{bmatrix} L & 0 & 0 & 0 \\ 0 & \sqrt{MPL^3} & 0 & 0 \\ 0 & 0 & P & 0 \\ 0 & 0 & 0 & P \end{bmatrix},$$

and the input transformation $u_* = (1/U)u$ with $U = (\sqrt{L^7/M})/C =: U_2$. Then, via a procedure similar to the one in the proof of Proposition 1, we obtain one of the other nondimensional representations:

$$\Sigma_2 \begin{cases} \ddot{s}^* = -D^*\dot{s}^* + A_+^* p_+^* - A_-^* p_-^* \\ \dot{p}_+^* = \dfrac{b^*}{1/2+s^*}\left(-\dot{s}^* + \dfrac{1}{A_+^*}Q_+^*\right) \\ \dot{p}_-^* = \dfrac{b^*}{1/2-s^*}\left(+\dot{s}^* - \dfrac{1}{A_-^*}Q_-^*\right) \end{cases} \tag{10}$$

and

$$Q_+^* = B^*(p_+^*, +u^*)u^*, \quad Q_-^* = B^*(p_-^*, -u^*)u^* \tag{11}$$

with

$$B^*(r,u^*) := \begin{cases} \sqrt{-r+1} & (u^*>0) \\ 0 & (u^*=0) \\ \sqrt{+r-0} & (u^*<0) \end{cases}$$

in which $D^* := D/\sqrt{MPL}$, $A_+^* := A_+/L^2$, $A_-^* := A_-/L^2$, $b^* := b/P$ □

Now, the other nondimensionalization (10) (11) also preserves the parameter structure in the original representation (1) (2). Indeed, by dropping the superscript $\bullet^*$, the other nondimensional representation (10) (11) can be equal to an original representation (1) (2) when $\theta = (1, D, 1, A_+, A_-, b, 1, 1)$. The nondimensional energy of the other nondimensional representation (10) (11) described by

$$\begin{aligned} H^* &= (1/2)(v^*)^2 \\ &\quad -(1/2+s^*)(b^*+p_+^*)A_+^* \\ &\quad -(1/2-s^*)(b^*+p_-^*)A_-^*, \end{aligned}$$

can be a special case of the original energy H.

The fourth advantage of the proposed nondimensional representation is the visualization. A difference between the nondimensionalizations in Proposition 1 and Example 2 is the dimension of the parameter space. Of course, the 4-dimensional parameter space with $(D^*, A_+^*, A_-^*, b^*) \in \mathbb{R}_+^4$ is much smaller than the original 8-dimensional parameter space $\mathbb{R}_+^8$ and close to the proposed 3-dimensional parameter space with $\theta^* = (D^*, A^*, P^*)$. However, only the proposed 3-dimensional parameter space can be visualized in 3D whereas even the 4-dimensional parameter space cannot.

IV. 3D VISUALIZATION

Not the accuracy but the new simplicity is evaluated in terms of the efficiency (parameter space reduction, verification-free, and fast computation) and visualization.

A. The numerical existence and nonlinearity

For many practical nonlinear systems, one of the most fundamental properties may be the stability [30] as long as the state exists. Especially, it is relevant that the state $x(t)$ exists within an restricted region: $\Omega_{LP} = (-L/2, L/2) \times \mathbb{R} \times [0, P]^2$ in the presence of the input. In addition to the numerical existence, the nonlinearity (or the input-output linearity) is also of interest for the linearization based controls [31] [7].

The numerical existence is evaluated by the existence of the escape time t_e [30] at which the state $x(t_e)$ starting from a test initial state $x(0) = (0, 0, P/2, (A_+/A_-)P/2)^{\mathrm{T}} \in \Omega_{LP}$ leaves the region Ω_{LP} for the first time in the presence of a test signal $u(t) = A_u \sin(2\pi f_u t)$ in the test period $[0, T_u]$. The numerical existence is achieved only if the escape time $t_e \in [0, T_u]$ does not exist. The numerical existence depends on the setting of the test parameters A_u, f_u, and T_u as well as $\theta = (M, D, L, A_+, A_-, b, C, P)$ and $x(0)$.

The nonlinearity is evaluated by a difference between an output of the nominal model and that of the linearized model:

$$\hat{\Sigma}_0 \begin{cases} M\dfrac{d^2\hat{s}}{dt^2} = -D\dfrac{d\hat{s}}{dt} + A_+\hat{p}_+ - A_-\hat{p}_- \\ \dfrac{d\hat{p}_+}{dt} = bV_+(0)^{-1}\left[-A_+\dfrac{d\hat{s}}{dt} + Q_+(P/2, u)\right] \\ \dfrac{d\hat{p}_-}{dt} = bV_-(0)^{-1}\left[+A_-\dfrac{d\hat{s}}{dt} - Q_-(P/2, u)\right] \end{cases} \tag{12}$$

whose state $\hat{x}(t) := (\hat{s}(t), \dot{\hat{s}}(t), \hat{p}_+(t), \hat{p}_-(t))^{\mathrm{T}}$ starts from the same state $\hat{x}(0) = x(0)$ in the presence of the same input $u(t)$. The displacement $s(t)$ and the driving force $f(t) = A_+p_+(t) - A_-p_-(t)$ are relevant in control [1] [7] whereas the pressures $p_\pm(t)$ are used in parameter identification [15]. Here, the difference is defined as the FIT ratio [32]:

$$\mathrm{FIT}(y_0^i) = \left(1 - \frac{\sqrt{\sum_{t=0}^{T_e}(\hat{y}_0^i(t) - y_0^i(t))^2}}{\sqrt{\sum_{t=0}^{T_e}(y_0^i(t) - \bar{y}_0^i)^2}}\right) \times 100$$

where $\bar{y}_0^i$ is the mean value of the i-th element $y_0^i(t)$ ($i = 1, \cdots, 4$) of the outputs $y_0(t) := (p_+(t), p_-(t), f(t), s(t))^{\mathrm{T}}$ of the nominal model and $\hat{y}_0^i$ is the i-th element of the corresponding outputs $\hat{y}_0(t) := (\hat{p}_+(t), \hat{p}_-(t), \hat{f}(t), \hat{s}(t))^{\mathrm{T}}$ of the linearized model (12). The results on the velocity $v(t)$ can be discussed by that on the displacement $s(t)$. If the numerical existence is achieved, $T_e := T_u$, otherwise $T_e := t_e \in [0, T_u]$. The value of $\mathrm{FIT}(y_0^i)$ can be negative.

B. Experimental conditions

The nonlinear dynamics computation and the parameter updates were repeated in the proposed nondimensional representation instead of the original representation. For the nonlinear dynamics computations, the equation (9) was applied to compute the nondimensional state $x^*(t^*)$ starting from the initial state $x^*(0) = (0, 0, P^*/2, A^*P^*/2)^{\mathrm{T}}$ in the presence of the test signal $A_u^* \sin(2\pi f_u^* t^*)$ with the amplitude $A_u^* := A_u/U_s = 0.01$ and the frequency $f_u^* := T_s f_u \in [0.001, 10]$. The test period was defined as $[0, T_u^*] := [0, 5/f_u^*]$. The modified backward differential formula with the variable step was applied (20-sim, Ver. 4.1, 64-bit 2.60GHz CPU with 8GB of memory). The nondimensional outputs $y_0^*(t^*)$ were given by the nondimensional state $x^*(t^*)$ directly. Using a similar procedure, the corresponding estimated outputs $\hat{y}_0^*(t^*)$ were also given by linearized model (12) in the nondimensional version. The damping constant, the rod area, and the source pressure $(D^*, A^*, P^*) \in [D_{\min}^*, D_{\max}^*] \times [A_{\min}^*, A_{\max}^*] \times$

$[P^*_{\min}, P^*_{\max}] = [0.0006, 11.2] \times [0.5, 1.0] \times [1.4 \times 10^{-5}, 0.07]$ were updated with the increments $\delta^*_D = 1.12$, $\delta_{A^*} = 0.05$, and $\delta_{P^*} = 0.007$, respectively and the other parameters $(M, A_+, L, b, C) = (1, 1, 1, 1, 1)$ were not updated.

C. Experimental results and discussion

Figure 3 shows the numerical existence and nonlinearity visualized in $D^*A^*P^*$ space. In the colorless regions on the slices, the numerical existence is not achieved since the escape time $t^*_e \in [0, T^*_u]$ exists such that $x^*(t^*_e) \notin \Omega_{1P^*}$. Figure 4 shows the time response examples corresponding to Figure 3 in the following four cases:
CASE-a: $(D^*, A^*, P^*) = (0.0006, 0.5, 0.07)$,
CASE-b: $(D^*, A^*, P^*) = (0.0006, 0.9, 0.07)$,
CASE-c: $(D^*, A^*, P^*) = (6.0, 0.5, 0.07)$,
CASE-d: $(D^*, A^*, P^*) = (6.0, 0.9, 0.07)$.
The outputs $y^*_0(t^*)$ are depicted as the curves. The maximum variable step was 10^4 times larger than the minimum one.

The numerical existence was not achieved when $A^* \leq 0.5$ at every frequency f^*_u. When $0.5 < A^* \leq 1.0$, the numerical existence depended on the frequency f^*_u. In particular, at the low frequency $f^*_u \leq 0.001$, the numerical existence was not achieved for $0.07 \leq P^*$. This may not be surprising in the sense that P^* increases only the gain of the nondimensional transfer function matrix:

$$\frac{\sqrt{8P^*}}{p^2 + D^*p + 2(1 + A^*)} \begin{bmatrix} (+p^2 + D^*p - 2(1 - A^*))/(2p) \\ (-p^2 - D^*p - 2(1 - A^*))/(2A^*p) \\ p + D^* \\ 1/p \end{bmatrix}$$

from the input u^* to the estimated outputs $\hat{y}^*_0 = (\hat{p}^*_+, \hat{p}^*_-, \hat{f}^*, \hat{s}^*)^{\mathrm{T}}$ of the linearized model (12) in the nondimensional version. The increase of P^* corresponds to the increase of the amplitude of the test signal. Here, the notation p denotes the derivative operator in the Laplace transform with respect to the nondimensional time $t^*(= t/T_s)$. Indeed, in Figure 4(a), there always exists $t^*_e \leq 450$ such that $x^*(t^*_e) \notin \Omega_{1P^*}$ due to the displacement saturation $s^*(t^*_e) \to +0.5$. Additionally, around the resonance frequency $\hat{f}^*_r(D^*, A^*) := \sqrt{2(1 + A^*) - (D^*/2)^2}/(2\pi) \in (0, 1/\pi)$ of the linearized model when the under-damping $(D^* < 2\sqrt{2(1 + A^*)} \in (2\sqrt{2}, 4]$, the numerical existence was not always achieved. In Figure 4(f), there exists $t^*_e \leq 6.5$ such that $x^*(t^*_e) \notin \Omega_{1P^*}$ due to the pressure saturation $p^*_-(t^*_e) \to P^*$ in CASE-a.

The colored regions on the slices in Figure 3 depict the FIT ratio as the nonlinearity. In Figure 5 which corresponds to Figure 4 the estimated outputs $\hat{y}^*_0(t^*)$ are depicted as the curves. For the pressures $p^*_\pm(t)$, remarkably, around a frequency $f^*_u = 0.02$, the lower nonlinearity (higher linearity) was achieved uniformly in $D^*A^*P^*$ space. This was observed as the time-response examples in Figure 4(d) and Figure 5(d). At other frequencies, the pressures $p^*_\pm(t^*)$ and the estimated ones $\hat{p}^*_\pm(t^*)$ could be very different as shown in Figure 4(b) and Figure 5(b) in spite of the best initial condition $p^*_\pm(0) = \hat{p}^*_\pm(0)$. In Figure 2, these nonlinearities, the non-negative and multi-peak pressures in CASE-c of Figure 4(b), were already observed.

For the driving force $f^*(t^*) = p^*_+(t^*) - A^*_- p^*_-(t^*)$, the lower nonlinearity was achieved at every frequency f^*_u in $D^*A^*P^*$ space uniformly. Figure 4(c) and Figure 5(c) show the corresponding time response examples. Interestingly, even when the pressures $p^*_\pm(t^*)$ and the estimated ones $\hat{p}^*_\pm(t^*)$ were very different, the force $f^*(t^*)$ could be approximated roughly by the estimated one $\hat{f}^*(t^*)$. At every high frequency $10 < f^*_u$, not only the pressure changes $p^*_\pm(t^*)$ but also the force $f^*(t^*)$ were small as shown in Figure 4(h) and Figure 5(h) and the nonlinearity was less important.

For the displacement $s^*(t^*)$, the nonlinearity was not uniform in $D^*A^*P^*$ space and also sensitive to the frequency f^*_u. The lower nonlinearity was achieved at every frequency f^*_u when $0.9 < A^* \leq 1.0$. As shown in Figure 4(b) and Figure 4(c), as long as $A^* \neq 1.0$, the displacement $s^*(t^*)$ could be asymmetric and was not always approximated by the estimated one $\hat{s}^*(t^*)$ which was more symmetric. At a glance, one may think that such asymmetric displacements were generated by a nonlinear friction effect. This conjecture is not true because the nominal model ignores the nonlinear friction effect. At every high frequency $0.1 \leq f^*_u$ except around the resonance frequency $\hat{f}^*_r(D^*, A^*)$, the displacement $s^*(t^*)$ was small as shown in Figure 4(h) and Figure 5(h) and the nonlinearity was again less important.

In all, at every frequency f^*_u, the linearization was roughly reliable for the driving force $f^*(t^*)$ in all cases and also for the displacement $s^*(t^*)$ when $0.9 \leq A^* \leq 1.0$. For the pressures $p^*_\pm(t^*)$, the linearization was roughly reliable around the frequency $f^*_u = 0.02$ in all cases. Precisely speaking, even for the driving force $f^*(t^*)$, the asymmetric nonlinearity existed as long as $A^* \neq 1.0$ and will affect the force and position control performance via the linearization. The verification-free and the visualization were successfully evaluated.

Remark 2 (Relating to parameter perturbation) Every parameter perturbation in the original parameter space (e.g. $b \to b(1 + \delta_b)$) can also be the perturbation in $D^*A^*P^*$ space (e.g. $D^* \to D\sqrt{L/(Mb(1 + \delta_b)A_+)} =: D^*(1 + \delta_{D^*})$, $P^* \to P/(b(1 + \delta_b)) =: P^*(1 + \delta_{P^*})$) by which a point in $D^*A^*P^*$ space is mapped into the other point. Note that the nonlinearity (color) at these points in Figure 3 evaluates uncertainty for the linearized model (12) and is different from uncertainty for the nominal model discussed in Remark 1.

For the numerical study to clarify comprehensive relations between the nonlinear dynamics and the many physical parameters, the proposed nondimensional representation has only $O(n^3)$ time complexity whereas the original representation has $O(n^8)$ time complexity. Since our experimental condition

TABLE I
COMPUTATION SPEED COMPARISON

Frequency f^*_u[1]	Computation time [s] in original representation	Computation time [s] in proposed representation
0.001	6942	3131
0.002	9028	4777
0.003	8242	3909
0.02	3295	1722
0.1	1675	841
0.3	1205	572
0.5	695	486
10	374	272

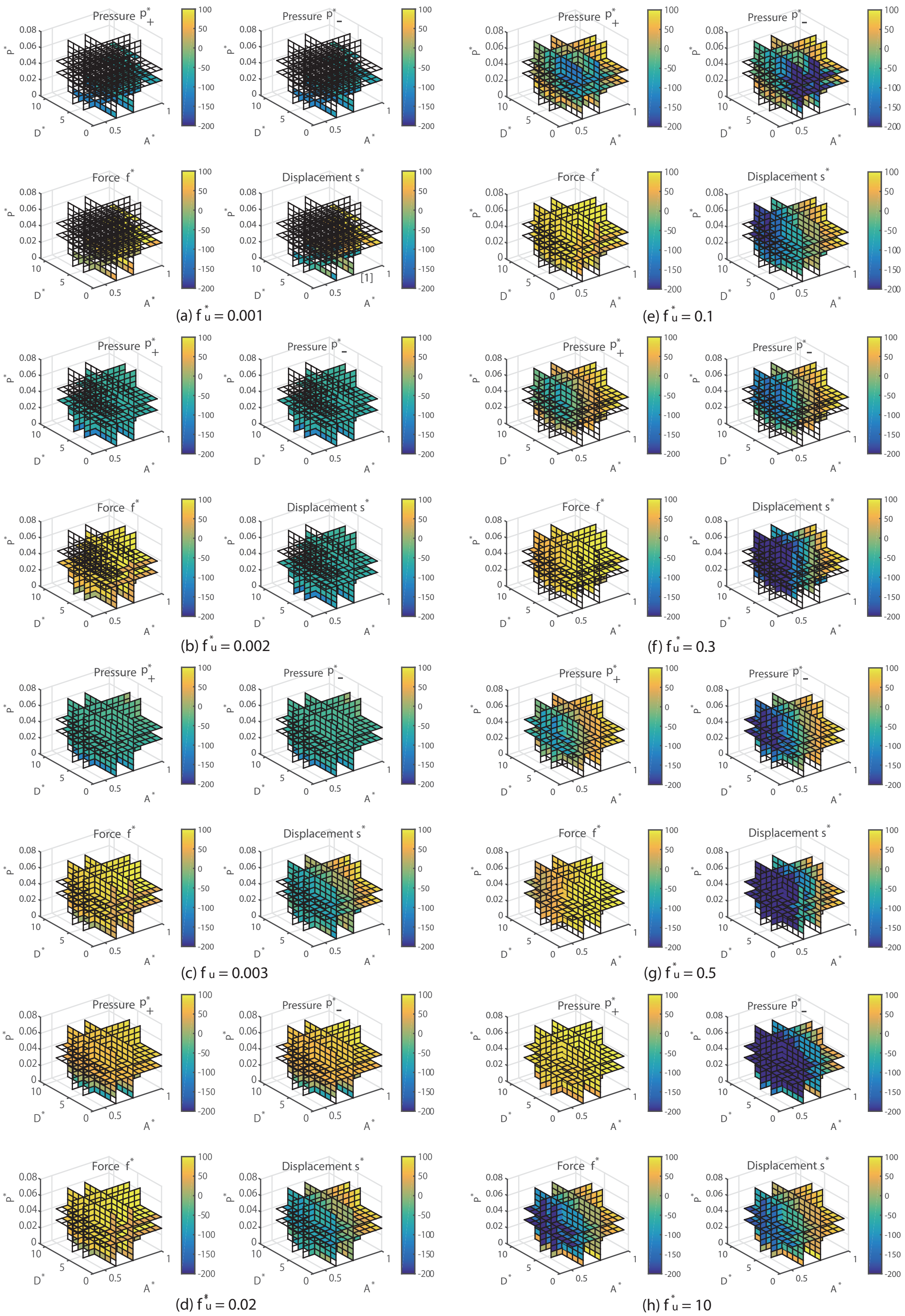

Fig. 3. Numerical existence and nonlinearity in $D^* A^* P^*$ space

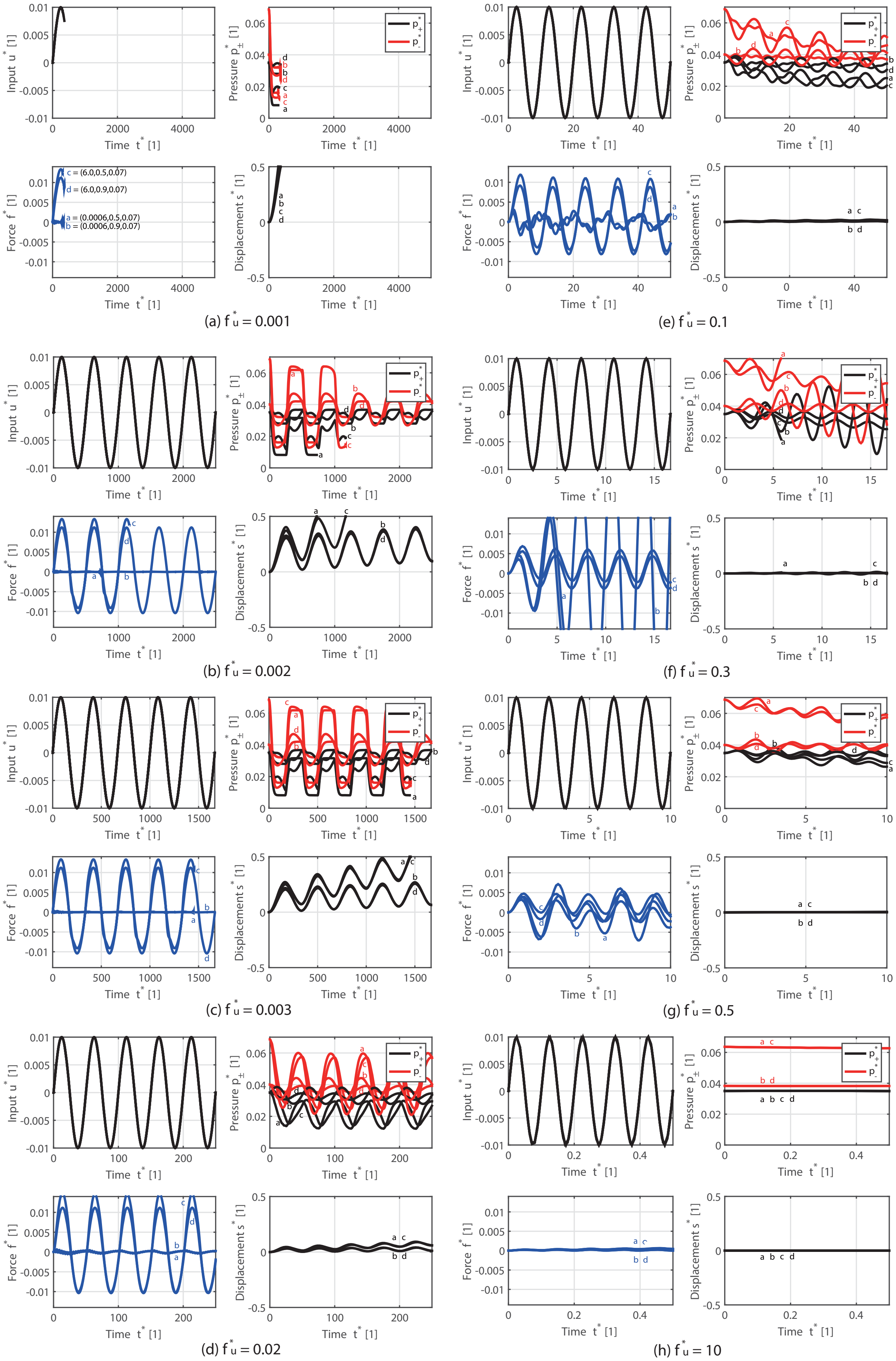

Fig. 4. Nondimensional time response (Nominal model)

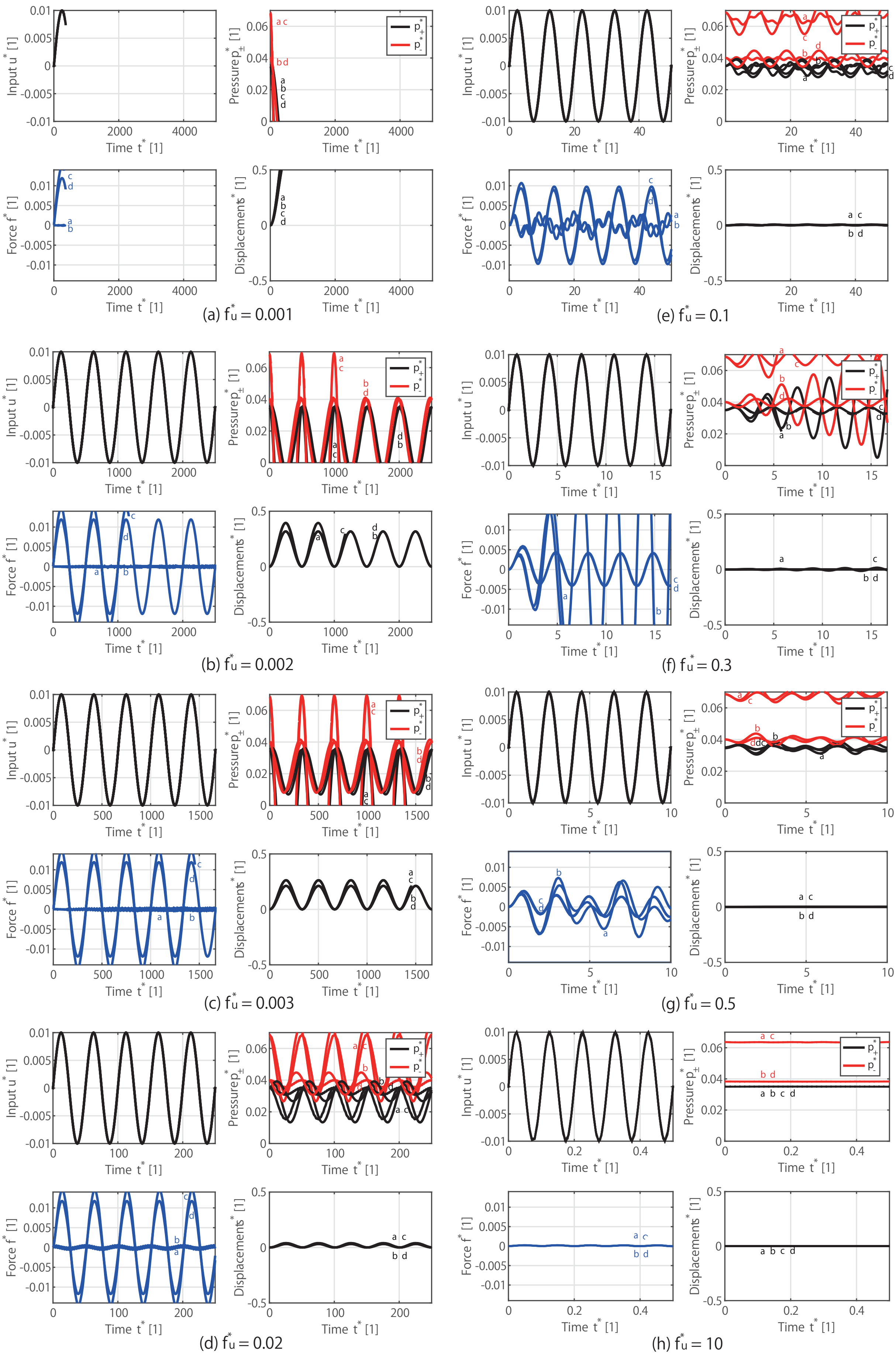

Fig. 5. Nondimensional time response (Linearized model)

took $n = 10$ to make Figure 3, the number of updates of the physical parameters was remarkably reduced. For the design optimization [8] which is not our main objective in this paper, since we may need the 5-dimensional search after the 3-dimensional search, the proposed nondimensional representation has $O(n^3) + O(n^5)$ time complexity at maximum which is still better than $O(n^8)$ time complexity even at $n = 2$. The parameter space reduction was also evaluated.

Table 1 evaluates the nonlinear dynamics computation time which is the sum of all computation times within $D^*A^*P^*$ space needed to make Figure 3. At every frequency f_u^*, as expected, the computation time for $x(t) = X_s\phi[\theta^*_{\text{special}}(\theta), x^*(0), u^*(t/T_s)]$ using the proposed nondimensional representation (3) (4) was better than that for $x(t) = \phi[\theta, x(0), u(t)]$ using the original representation (1) (2). In total, the computation time of the proposed nondimensional representation was reduced to 15710 s (4.2 h) which is around the half of that of the original representation 31455 s (8.7 h). This is because the parameters $(M, A_+, L, b, C) = (1, 1, 1, 1, 1)$ reduce the number of multiplication and division operations preserving the parametric structure in the original representation (1) (2). The computation time can be improved more since all existing methods [8] [33] developed for the original representation (1) (2) can be applied. While the computations were made for only eight frequencies f_u^* in Table 1, the fast computation was well evaluated.

Finally, let us remark that Proposition 1 and Theorem 1 provide the links to the closed-loop discussion as well as the open-loop discussion presented in the above of this paper.

Remark 3 (Relating to design and control via scaling) Let us put a simple example of the links based on our experimental 1-DOF arm, and consider a scaling design and control problem of a hydraulic cylinder whose piston undershoot should be zero in the presence of force disturbance. Assume that only $(D, A_+, b) = (11000\ \mathrm{Ns/m}, 0.0021\ \mathrm{m}^2, 5.3 \times 10^8\ \mathrm{Pa})$ are given and the others $(M, L, A_-, C, P) \in \mathbb{R}^5_+$ and a gain $F > 0$ of the simple control $u(t) = -Fs(t)$ are unknown under a certain working constraints $L/2 \geq 2.5\ \mathrm{m}$ (with pipeline length effect), $A_- \leq 0.0016\ \mathrm{m}^2$, $P \leq 21 \times 10^6\ \mathrm{Pa}$ in the large scale.
[Step 1] In the large scale, we search the parameters (M, L, A_-, C, P) by the advanced direct search approach. Since the transfer function in the following linearization based control (the classical control) does not treat any initial response $\bar{x}(t) := \phi[\theta, x(0), u(t) \equiv 0]$, the objective function is the norm overshoot $\max_{0 \leq t < \infty} |\bar{x}(t)^{\mathrm{T}} Q \bar{x}(t)|$ by the random initial state $x(0) \in \Omega_{LP}$. Here, we will suffer from $O(n^5)$ time complexity without Proposition 1 and Theorem 1, but now only $O(n^3)$ time complexity is needed. when $n = 10$ and $Q = \mathrm{diag}(1, 1, 0.1, 0.1)$, the searched parameters are $(D^*, A^*, P^*) = (4.1, 0.75, 0.028)$ which imply $(M, L, A_-, C, P) = (M, 0.144M, 0.0016\ \mathrm{m}^2, C, 14 \times 10^6\ \mathrm{Pa})$ with the free parameters M and C. Under the constraints, our choice is $M = 100$ kg and $C = 1.8 \times 10^{-4} \sqrt{\mathrm{m}^5/\mathrm{kg}}$. The physical units are unique and dropped in the following.
[Step 2] In the large scale, we prepare the linearization based control $u(t) = -Fs(t)$ whose nondimensional version is $u^*(t^*) = -(1/U_s)F(Ls^*(t^*)) =: F^*s^*(t^*)$. By the standard linear analysis, if $F^* < \{-(2(D^* - 6(1 + A^*))^{3/2})/27 + 2(D^*)^3/27 - 2D^*(1 + A^*)/3\}/\sqrt{8P^*} \approx 1.82$, the zero-undershoot is guaranteed for the linearized model (12), but not guaranteed for the nominal model due to the nonlinearity. Figure 6 shows the disturbance responses (the solid black and red curves) with $F = 0.0128$ $(F^* = 0.908 < 1.82)$ of the nominal model and that of the linearized model (12) against the step disturbance 20000 N. Fortunately, without adjusting F, the zero-undershoot for the nominal model is confirmed numerically (not analytically) whereas the response (the dashed red curve) with $F = 0.0345$ $(F^* = 2.45 > 1.82)$ has the nonzero (dangerous) undershoot for the linearized model (12). The response difference between the models with the same gain corresponds to the nonlinearity (the FIT ratio ≈ 0 in the band $f_u^* < 0.02$) in Figure 3 which justifies to use the nominal model instead of the linearized model (12).
[Step 3] In a certain small scale, we design and control the small scaled hydraulic cylinder since the similarity [34] is sometimes required to reduce the experimental cost in the large scale. Here, by replacing $M = 100 \to 25$ and keeping (D^*, A^*, P^*) and F^*, we have $(M, L, A_-, C, P) = (25, 3.6, 0.0016, 1.8 \times 10^{-4}, 14 \times 10^6)$ and $F = 0.0512$. Against the nonlinearity, based on Proposition 1 and Theorem 1, the zero-undershoot is guaranteed even for the nominal model in the small scale. Indeed, Figure 6 shows no undershoots in the disturbance responses with $F = 0.0512$ of both models in the small scale. Now we can start to construct the small scaled hydraulic cylinder for the experimental validation.

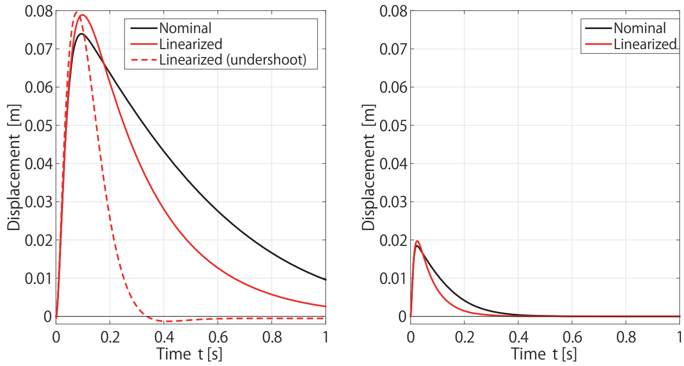

Fig. 6. Disturbance response (Left: large scale, Right: small scale).

V. Conclusion

This paper reveals that a nominal model of hydraulic cylinders has a new simplicity on the parametric structure that more accurate or complex, and merely simple existing models do not have. Without loss of generality, only by changing the damping constant D^*, the rod area A^*, and the source pressure P^* and assuming that all the other physical parameters are unity, any index, such as the numerical existence and nonlinearity, is visualized efficiently. Three parameters D^*, A^*, and P^* correspond to the damping parameter d^* of the mass-damper-spring, or to the Froude number Fr and the Reynolds number Re of the fluid system in Section I. This is an inevitable, unexpected, and economical result. Roughly speaking, Figure 4 is the best possible result corresponding to the analytical (analytic) solution. In this sense, the comprehensive relations between the nonlinear dynamics and many physical parameters are clarified. Besides the small and large scale experiments, one of the key future works is to improve the accuracy of the nominal model keeping the simplicity for control.

REFERENCES

[1] Jouni Mattila, Janne Koivumaki, Darwin G. Caldwell, and Claudio Semini. A Survey on Control of Hydraulic Robotic Manipulators with Projection to Future Trends. IEEE/ASME Transactions on Mechatronics, 22(2):669-680, 2017.

[2] Shan Chen, Zheng Chen, Bin Yao, Xiaocong Zhu, Shiqiang Zhu, Qingfeng Wang, and Yang Song. Adaptive robust cascade force control of 1-DOF hydraulic exoskeleton for human performance augmentation. IEEE/ASME Transactions on Mechatronics, 22(2):589-600, 2017.

[3] Jianyong Yao, Zongxia Jiao, and Dawei Ma. A practical nonlinear adaptive control of hydraulic servomechanisms with periodic-like disturbances. IEEE/ASME Transactions on Mechatoronics, 20(6):2752-2760, 2015.

[4] T. Boaventura, M. Focchi, M. Frigerio, J. Buchli, C. Semini, G. A. Medrano-Cerda, and D. G. Caldwell. On the role of load motion compensation in high-performance force control. In Proc. IEEE/RSJ IROS, pages 4066-4071, 2012.

[5] M. Jelali and A. Kroll. Hydraulic Servo Systems. Springer, 2002.

[6] H. Merritt. Hydraulic Control Systems. John Willey and Sons, 1967.

[7] S. Sakai, K. Osuka, T. Maekawa, and M. Umeda. Robust control systems of a heavy material handling agricultural robot: A case study for initial cost problem. IEEE Transactions on Control Systems Technology, 15(6):1038-1048, 2007.

[8] S. Sakai. Casimir based fast computation for hydraulic robot optimizations. In Proc. IEEE/RSJ IROS, pages 2874-2881, 2013.

[9] I. Nezu and H. Nakagawa. Turbulence in Open Channel Flows. CRC Press, 1993.

[10] J. Nurmi and J. Mattila. Detection and isolation of leakage and valve faults in hydraulic systems in varying loading condition, part 1: Global sensitivity analysis. International Journal of Fluid Power, 12:41-51, 2011.

[11] M. Vilenius. Application of sensitivity analysis to electrohydraulic position servos. ASME Journal of Dynamic Systems, Measurements and Control, 106:77-82, 1984.

[12] G. Grabmair and K. Schlacher. Energy-based nonlinear control of hydraulically actuated mechanical systems. In Proc. of IEEE CDC, pages 7520-7525, 2005.

[13] A. Kugi and W. Kemmetmuller. New energy-based nonlinear controller for hydraulic piston actuators. European Journal of Control, 10:163-173, 2004.

[14] P. Y. Li and M. R. Wang. Natural storage function for passivity-based trajectory control of hydraulic actuators. IEEE/ASME Transactions on Mechatoronics, 19(3):1057-1068, 2014.

[15] S. Sakai and Y. Maeshima. A new method for parameter identification for N-dof hydraulic robots. In Proc. of IEEE ICRA, pages 5983-5989, 2014.

[16] K. Zhou, J. C. Doyle, and K. Glover. Robust and Optimal Control. Prentice-Hall, 1996.

[17] A. J. van der Schaft. L2-Gain and Passivity Techniques in Nonlinear Control. Springer-Verlag, 2000.

[18] E. Buckingham. On physically similar systems. Physics review, (4):354-376, 1931.

[19] W. D. Curtis, J. David Logan, and W. A. Parker. Dimensional analysis and the pi theorem. Linear Algebra and Its Applications, (47):117-126, 1982.

[20] K. Fujimoto and T. Sugie. Canonical transformation and stabilization of generalized Hamiltonian systems. Systems and Control Letters, 42(3):217-227, 2001.

[21] J. Watton. Fluid Power Systems. Prentice-Hall, 1989.

[22] B. M. Maschke, A. J. van der Schaft, and P. C. Breedveld. An intrinsic Hamiltonian formulation of network dynamics: Non-standard Poisson structures and gyrators. Journal Franklin Institute, 329:923-966, 1992.

[23] A. J. van der Schaft and B. M. J. Maschke. The Hamiltonian formulation of energy conservation physical systems and external ports. In Archivfur Electronic und Ubertrangungstechnik, 49:362-371, 1995.

[24] V. Duindam, A. Macchelli, S. Stramigioli, and H. Bruyninckx. Modeling and Control of Complex Physical Systems: The Port-Hamiltonian Approach. Springer, 2009.

[25] S. Stramigioli, C. Secchi, A. van. der. schaft Schaft, and C. Fantuzzi. Sampled data systems passivity and discrete port-Hamiltonian systems. IEEE Trans. on Robotics, 21(4):574-587, 2005.

[26] K. Fujimoto and T. Sugie. Iterative learning control of Hamiltonian systems: I/O based optimal control approach. IEEE Transactions on Automatic Control, 48(10):1756-1761, 2003.

[27] M. R. Sirouspour and S.E. Salcudean. Nonlinear control of hydraulic robots. IEEE Transactions on Robotics and Automation, 17(2):173-182, 2001.

[28] S. Sakai. A special structure preserving nondimensionalization of hydraulic rotational joints. In Proc. of IEEE ICRA, page 26-32, 2017.

[29] T. Yoshikawa. Foundation of Robotics. MIT Press, 1990.

[30] H. K. Khalil. Nonlinear Systems. Prentice-Hall, 1996.

[31] B. Heinrichs, N. Sepehri, and A. B. Thornton-Trump. Position-based impedance control of an industrial hydraulic manipulator. IEEE Control Systems Magazine, 17(1):46-52, 1997.

[32] L. Ljung. System Identification: Theory for the User. Prentice-Hall, 1999.

[33] S. Sakai and S. Stramigioli. Passivity based control of hydraulic robot arms using natural Casimir functions. In Proc. of IEEE/RSJ IROS, pages 538-544, 2008.

[34] V. I. Arnold. Mathematical Methods of Classical Mechanics. Springer-Verlag, 1989.

PLACE PHOTO HERE

Satoru Sakai Satoru Sakai received the B.E. degree in Engineering and the M.E. and Ph.D. degrees in Agricultural Engineering from Kyoto University, Japan, in 1998, 2000 and 2003, respectively. In 2005, he joined Chiba University. In 2010, he joined Shinshu University, Japan, where he is currently an associate professor with the Department of Mechanical Engineering. From 2003 to 2005, he was a JSPS postdoctoral research fellow with the Department of Informatics, Kyoto University, and from 2004 to 2005 he was a visiting researcher with the Faculty of Electrical Engineering, University of Twente, Netherlands. His research interests include robotics, systems & control. He was a recipient of the Young Author Prize at IFAC 2005.

PLACE PHOTO HERE

Stefano Stramigioli Stefano Stramigioli received the M.Sc. (Hons.) degree (cum laude) from the University of Bologna, Bologna, Italy, in 1992 and the Ph.D. (Hons.) degree (cum laude) from the Delft University of Technology, Delft, The Netherlands, in 1998. He is currently a Full Professor of advanced robotics and the chair holder of the Robotics and Mechatronics Group, University of Twente. He has more than 200 publications including four books. He is currently the Vice-President for Research of euRobotics, the private part of the PPP with the EU known as SPARC. He has been an Officer and AdCom Member for IEEE/RAS.